Localization and roles of Ski8p protein in Sordaria meiosis and delineation of three mechanistically distinct steps of meiotic homolog juxtaposition

Sophie Tessé*, Aurora Storlazzi*†, Nancy Kleckner‡§, Silvana Gargano†, and Denise Zickler*

*Institut de Génétique et Microbiologie, Université Paris-Sud, 91405 Orsay Cedex, France; ‡Department of Molecular and Cellular Biology, Harvard University, 7 Divinity Avenue, Cambridge, MA 02138; and †Istituto di Genetica e Biofisica, A. Buzzati Traverso, Consiglio Nazionale delle Ricerche, Via Marconi 10, 80125 Naples, Italy

Contributed by Nancy Kleckner, June 30, 2003

Ski8p is implicated in degradation of non-poly(A) and double-stranded RNA, and in meiotic DNA recombination. We have identified the *Sordaria macrospora* SKI8 gene. Ski8p is cytoplasmically localized in all vegetative and sexual cycle cells, and is nuclear localized, specifically in early-mid-meiotic prophase, in temporal correlation with Spo11p, the meiotic double-strand break (DSB) transesterase. Localizations of Ski8p and Spo11p are mutually interdependent. *ski8* mutants exhibit defects in vegetative growth, entry into the sexual program, and sporulation. Diverse meiotic defects, also seen in *spo11* mutants, are diagnostic of DSB absence, and they are restored by exogenous DSBs. These results suggest that Ski8p promotes meiotic DSB formation by acting directly within meiotic prophase chromosomes. Mutant phenotypes also divide meiotic homolog juxtaposition into three successive, mechanistically distinct steps; recognition, presynaptic alignment, and synapsis, which are distinguished by their differential dependence on DSBs.

Meiosis is characterized by a high level of genetic recombination. During early prophase, many recombinational interactions are initiated, some of which mature into crossovers. Crossovers, in combination with sister chromatid arm connections, provide physical links between homologs that promote their accurate segregation at division I (1, 2).

Meiotic recombination is initiated by programmed double-strand breaks (DSBs), catalyzed by the Spo11p transesterase (3). In budding yeast, at least nine other genes are directly involved (3, 4). Three of these genes also play key roles in recombinational repair during mitosis (4); five others are meiosis specific. The ninth gene, *REC103/SKI8* (fission yeast ortholog *rec14*) is particularly intriguing, because it also plays a prominent role in cytoplasmic mRNA metabolism. Yeast *SKI* genes were originally identified as essential for controlling propagation of double-stranded RNA viruses (5). Ski8p, which forms a complex with Ski3p and Ski2p, is also required for 3′ to 5′ degradation of mRNA and repression of translation of nonpolyadenylated RNA (6–10). Ski8p contains several WD motifs thought to mediate protein–protein interactions (11, 12). Mutations in *SKI8* and *rec14* confer strong reductions in meiotic recombination but have no detectable effects on mitotic recombination or DNA repair (13–18). Given its RNA metabolism function, Ski8/Rec14p might promote meiotic recombination indirectly; e.g., through effects on expression of other DSB genes. However, Ski8p and Spo11p interact in two-hybrid assays (19), consistent with a direct effect.

Here, we report molecular identification of the *Sordaria macrospora SKI8* gene, cytological localization of Ski8p, and analysis of *ski8* mutant defects in the vegetative and sexual cycles. Meiotic defects and their amelioration by exogenous DSBs are described in detail.

Materials and Methods

Strains. All mutant strains are derived from the homothallic *Sordaria macrospora* St. Ismier strain, FGSC 4818. The *asy5/ski8* mutations were UV-induced (20). *SKI8-GFP* and *RAD51-GFP* contain the entire coding ORF fused to the GFP ORF from pEGFP-1 (Clontech). *SKI8* and *SKI8-GFP* alleles were introduced ectopically by selection for hygromycin resistance (21).

***SKI8* Cloning and Sequencing.** A cosmid clone containing *SKI8* was identified by PCR in an *S. macrospora* indexed genomic cosmid library (22), with primer design based on the *Neurospora crassa SKI8* genomic sequence (Whitehead Institute/Massachusetts Institute of Technology Center for Genome Research, Cambridge, MA; www-genome.wi.mit.edu). The Sordaria *SKI8* coding region was subcloned and sequenced. The *asy5/ski8* mutations were identified by the sequencing of both strands using gene-specific primers (Sigma Genosys, The Woodlands, TX), a Big Dye Terminator cycle sequencing kit (Applied Biosystems), and a 310 DNA sequencer (Applied Biosystems).

Cytology. Asci were processed for immunofluorescence, as described in ref. 23. The primary antibody was anti-Rad51 (Oncogene Science) at 1:400. Secondary antibodies were FITC or CyTM3 anti-rabbit (Jackson ImmunoResearch) at 1:100. Controls included primary or secondary antibodies alone. Chromatin was visualized with 4′,6-diamidino-2-phenylindole (DAPI) (0.5 μg/ml). Immunofluorescence and GFP fluorescence were observed on a Zeiss Axioplan microscope with a Princeton charge-coupled device camera, and a Zeiss LSM 510 confocal laser scanning microscope. Hematoxylin staining and light microscopy (LM) were as described (21). For electron microscopy (EM), asci were fixed, sectioned and visualized as in ref. 24. 3D rendering was constructed by VECTOR WORKS and ZOOM software.

Results

Sordaria *SKI8*: Cloning and Identification as *ASY5*. The *S. macrospora SKI8* gene was identified by analogy with the corresponding *N. crassa* gene (see *Materials and Methods*, GenBank accession no. AY363394). Previous studies (20) identified a unique Sordaria meiotic mutant, *spo76-1*, whose spore-formation defect is suppressed by mutations in seven genes. One of these genes is *SPO11* (25). Complementation studies now identify another of these genes, *ASY5*, as *SKI8* (data not shown). Genomic sequence analysis of five *asy5* alleles identifies specific corresponding mutations (see Fig. 7, which is published as supporting information on the PNAS web site, www.pnas.org).

***ski8* Mutants Are Altered in Vegetative Growth and Fruiting Body Development.** Vegetative growth was examined by placing an agar plug of young, growing mycelium at one end of a 35-cm-long tube

Abbreviations: ski, superkiller; SC, synaptonemal complex; AE, axial element; DSB, double-strand break; LM, light microscopy; EM, electron microscopy; DAPI, 4′,6-diamidino-2-phenylindole.

§To whom correspondence should be addressed. E-mail: kleckner@fas.harvard.edu.

and measuring its extension along the length of the tube over time. At 23°C, the normal temperature for Sordaria experiments, and at 32 and 6°C, WT mycelia grow at 1.9, 1.74, and 0.35 cm per day, respectively. All *ski8* mutants exhibit altered growth patterns. At 23°C, *ski8-22* and *ski8-7* grow slightly faster, and *ski8-33* slightly slower, than WT (see Fig. 8*A*, which is published as supporting information on the PNAS web site). At 32°C, in *ski8-7*, periods of rapid growth alternate with periods of slower, more dense growth, until growth finally ceases (Fig. 8 *B* and *C*). At 6°C, all *ski8* mutants grow slightly slower than WT, and then slow dramatically, like WT, except *ski8-7* (Fig. 8*D*). None of the five *ski8* mutants is sensitive to UV or X irradiation (data not shown).

The Sordaria sexual cycle occurs within fruiting bodies (perithecia), which arise along a tube of growing mycelia as a parallel wave, offset by 3 days (23°C) or 20 days (6°C). At 23°C, all *ski8* mutants, except *ski8-13*, show retarded perithecia formation. At 6°C, *ski8* mutants form only small and rare perithecia, and only after 25 days. At 32°C, neither WT nor mutants form perithecia.

A perithecium contains ≈200 asci (meiocytes), each issued from the fusion of two haploid nuclei. At 23°C, *ski8* mutants exhibit delayed ascus emergence. Karyogamy is also delayed, as seen by an elevated proportion of asci containing unfused nuclei (data not shown). In WT, chromosome axes-associated protein Spo76-GFP, is seen only at telomeres in prekaryogamy nuclei, and then all along the chromosomes at leptotene. Interestingly, in *ski8* mutants, full-length Spo76-GFP staining is seen also in prekaryogamy nuclei, suggesting that chromosome morphogenesis proceeds despite the delay in nuclear fusion. *ski8* mutants then proceed through the basic meiotic stages, but aberrantly (below). *ski8-22*, *ski8-33*, and *ski8-34* complete ascospore formation after 4 days, as in WT; *ski8*-7 completes sporulation 1 day late, and *ski8-13*, 1 day early, as with Sordaria *spo11*Δ (data not shown).

Ski8p Localizes to Chromosomes Specifically at Early-Mid-Meiotic Prophase, Contemporaneously with Spo11p. Ski8, tagged with GFP at its C terminus and present as an ectopic insert (see *Materials and Methods*), complements all *ski8* mutants, implying that it is functional, and does not confer any aberrant phenotype to WT. Ski8-GFP is visible in the cytoplasm at all vegetative and sexual cycle stages. Staining is brighter during vegetative growth (Fig. 1 *A* and *B*) and in developing ascospores than in asci and resting ascospores (data not shown). Ski8-GFP is also visible in nuclei, specifically during meiotic prophase. Staining is seen throughout the chromosomes from early leptotene through mid-pachytene, without any specific pattern, but brighter in leptotene (Fig. 1 *C* and *D*) than in pachytene (Fig. 1 *E* and *F*), and disappears at the end of pachytene. Ski8-GFP reappears specifically in nuclei of just membranated ascospores (Fig. 1 *G* and *H*).

Mutually Interdependent Localization of Ski8p and Spo11p. In a *spo11*Δ mutant, just as in WT, Ski8p exhibits cytoplasmic staining in all cell types, nuclear staining from leptotene to pachytene, and reappearance of staining in newly formed ascospores. However, the Ski8-GFP meiotic prophase nuclear signal is now faint (Fig. 1 *I* and *J*). In all *ski8* mutants, just as in WT, Spo11p is seen in nuclei only from leptotene to pachytene, and in young ascospores. However, whereas Spo11-GFP occurs as foci in chromatin at leptotene, and as lines from late leptotene through mid-pachytene in WT (Fig. 1 *K* and *L*), neither foci nor lines are observed in *ski8-7*, *-34*, *-13*, and *-33*. Instead, diffuse staining occurs throughout the chromosomes during this entire period (Fig. 1 *M* and *N*). In *ski8-22*, no Spo11 foci are seen at leptotene, but chromosome axes exhibit a light staining from bouquet through mid-pachytene. Thus, Ski8p and Spo11p do not require one another for correct timing of nuclear localization or ascospore staining, but do require one another for a correct pattern of localization to chromosomes during early-mid-meiotic prophase.

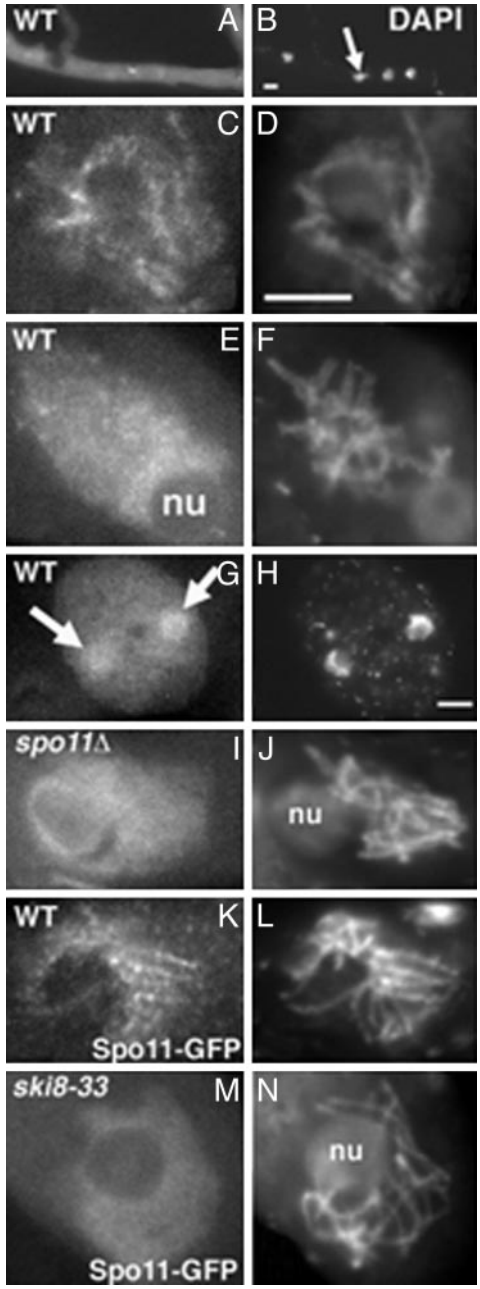

Fig. 1. Ski8 localization. (*A–H*) WT. (*A*) Mycelium with bright Ski8-GFP signal. (*B*) Corresponding DAPI with four nuclei (arrow). (*C*) Late leptotene nucleus with chromatin-associated Ski8-GFP. (*D*) Corresponding DAPI. (*E*) Late pachytene nucleus with diffuse Ski8 signal. (*F*) Corresponding DAPI. (*G*) Ascospore with two nuclei (arrows) stained by Ski8-GFP. Note also the bright cytoplasmic staining when compared with the ascus staining in *E*. (*H*) Corresponding DAPI. (*I*) Ski8-GFP staining in a *spo11*Δ prophase nucleus. (*J*) Corresponding DAPI. (*K*) Spo11-GFP staining in a WT bouquet nucleus. (*L*) Corresponding DAPI. (*M*) Spo11-GFP staining in a *ski8-33* leptotene nucleus. (*N*) Corresponding DAPI. nu, nucleolus. (Bar, 5 μm.)

Ski8p Is Required for Formation of Rad51 Foci and Chiasmata. Rad51p marks the sites of meiotic DSBs (e.g., ref. 26). When analyzed with antibodies against Rad51p, or by Rad51-GFP, WT nuclei exhibit foci on chromosomes from mid-leptotene to late zygotene, with maximum abundance from late leptotene through

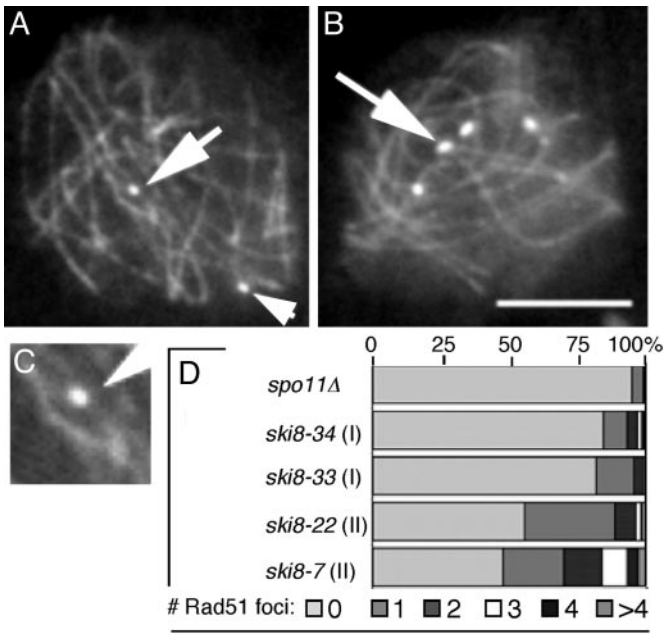

Fig. 2. Rad51p foci in *ski8* leptotene nuclei double-stained by Spo76-GFP and anti-Rad51 antibodies. (*A*) *ski8-33* with two foci (arrows). (*B*) *ski8-7* with six foci (arrow points to brighter dots). (*C*) Enlargement of upper Rad51 focus in *A*. (*D*) Distribution of focus numbers per nucleus in *ski8* mutants and *spo11*Δ. (Bar, 5 μm.)

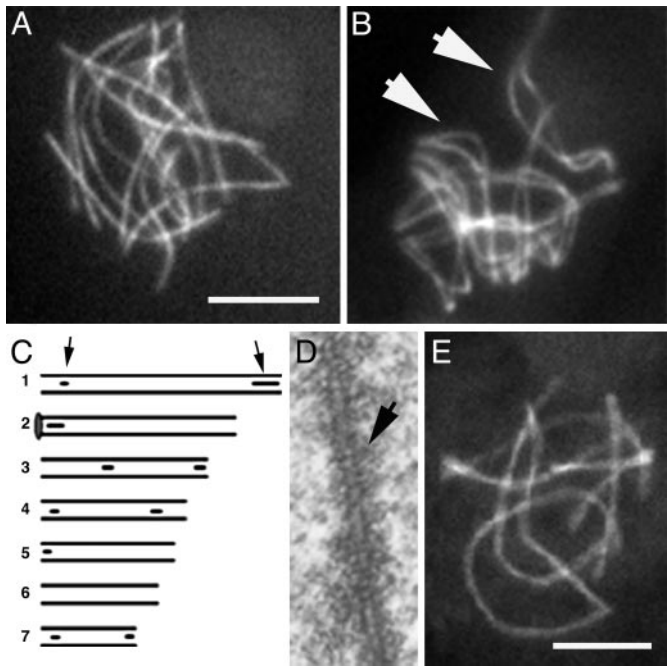

Fig. 3. Pairing and synapsis phenotypes of *ski8* mutants. (*A*) Type I *ski8-33* nucleus with only unpaired homologs. (*B*) Type II *ski8-22* nucleus with aligned homologs (arrows point to two bivalents). (*C*) EM-reconstructed *ski8-7* nucleus. Six of the seven homolog pairs show SC initiation sites (arrows point to bivalent 1, gray circle; bivalent 2 ends in nucleolus). (*D*) AE of *ski8-22* is doubled and striated (arrow). (*E*) *ski8-7* nucleus with seven synapsed bivalents. (Bars, 5 μm for LM; 1 μm for EM.)

early zygotene (≈55–60 foci per nucleus; $n = 150$). In all *ski8* mutants, Rad51 foci are rare (calculated from 250 prophase nuclei in each strain; Fig. 2). Two categories of *ski8* mutants are defined. In type I mutants (*ski8-33* and *ski8-34*), ≈85% of nuclei show no foci, and ≈15% show one to four foci (Fig. 2 *A*, *C*, and *D*). In type II mutants (*ski8-22* and *ski8-7*), more foci are seen, with ≈50% of nuclei exhibiting one to more than seven foci (Fig. 2 *B* and *D*). All *spo11*Δ *ski8* double mutants look like *spo11*Δ single mutants (Fig. 2*D*). *ski8* mutants exhibit correspondingly depressed frequencies of chiasmata. WT diplotene nuclei exhibit 21 ± 3 chiasmata (27). In type I mutants, chiasmata are rare (six nuclei with one to two chiasmata among 50 analyzed diplotenes). In type II mutants, chiasmata are more common. For example, among 50 diplotene *ski8-7* nuclei, ≈25% exhibit one to five chiasmata (data not shown).

***ski8* Mutants Exhibit Normal Axes/Axial Elements (AEs) but Rare Synapsis/Synaptonemal Complexes (SCs).** In all *ski8* mutants, leptotene chromosome axes develop normally. As in WT, Spo76p stains continuous chromosome axes from early prophase until the diffuse stage (Fig. 3 *A* and *B*). 3D EM reconstructions of 10 *ski8-7* and 10 *ski8-33* nuclei extend this observation. As in WT, (*i*) AEs are continuous along all chromosomes by mid-leptotene; (*ii*) all chromosome ends are anchored within the nuclear envelope; (*iii*) total AE length is similar to WT (81–89 μm versus 90 ± 6 μm); (*iv*) homologous pairs have the same AE lengths (Fig. 3*C*); (*v*) AEs are similarly striated in mutants as in WT (Fig. 3*D*); and (*vi*) AEs disappear at the diffuse stage. The only alteration in *ski8* AEs is that, at a stage corresponding to late pachytene in WT as judged by ascus size, they double and become thicker (Fig. 3*D*) over 22–70% of their lengths.

All *ski8* mutants are defective for SC formation (by EM) or synapsis (by LM). None of the 20 *ski8* mid-prophase nuclei reconstructed from EM serial sections showed complete SC formation. Only two *ski8-7* nuclei, at the stage analogous to WT pachytene by ascus size, showed some SCs, at telomere regions and interstitially (Fig. 3*C*), representing 9% and 12% of total WT SC length, respectively. No SCs were seen in the 18 other nuclei. Analyses of Spo76-GFP-stained nuclei (200 per mutant; three experiments) further reveal that type I mutants never show complete synapsis (Fig. 3*A*), whereas type II mutants show almost complete (Fig. 3*B*) or complete synapsis (Fig. 3*E*) in 10–15% of nuclei. All mutants exhibit some nonhomologous synapsis at late pachytene, as defined by ascus size (data not shown). AE and SC/synapsis characteristics of Type I *ski8* mutants are identical to those of *spo11* mutants (25).

Progressive Homolog Recognition and Pairing During WT Meiosis. In Sordaria, spatial relationships among different chromosomes are revealed by analysis of AEs in EM 3D reconstructions, and by confocal analysis of Spo76-GFP-stained axes (21, 24, 25). In early WT leptotene nuclei, AEs of homologs are far apart, with no evidence of any specific relationship (Fig. 4 *A–C*). By mid-leptotene, homologs have clearly moved and are now in rough long-range coalignment (Fig. 4*D*), as seen clearly when homologs are considered two by two (Fig. 4 *E* and *F*). All homolog pairs then come progressively into coalignment at a distance of ≈400 nm, initially segmentally, and ultimately, along their entire lengths (Fig. 4*G*). Shorter chromosomes are mostly aligned before longer chromosomes (Fig. 4 *E* and *F*). From early leptotene onward, chromosome ends are attached to the nuclear envelope. They are dispersed throughout the nuclear periphery (Fig. 4*A*), without localization to any specific regions, through the time of presynaptic coalignment (Fig. 4*D*). The same progression of stages, from mid-leptotene to presynaptic coalignment at late leptotene, is seen with Spo76-GFP (Fig. 4*H*); at earlier stages, nuclei are too tiny for LM analysis.

We also double-stained prophase nuclei for Spo76-GFP and for Rad51 (with antibodies or Rad51-GFP). Rad51 foci appear often between presynaptically aligned chromosomes (Fig. 4*I*), or on chromosome axes, in accord with plant studies and

immunoelectron microscope studies in mouse, which localize RecA homologs to bridges that link homolog axes at presynaptic coalignment distance (1, 28).

Presynaptically coaligned chromosomes then form a loose-bouquet configuration in which one or both ends of each chromosome are clustered in a limited area of the nuclear envelope, with concomitant initiation of SC formation (EM) and synapsis (LM) (Fig. 4*J*). SC initiates preferentially at the chromosome ends, but multiple interstitial initiations are seen, particularly in longer chromosomes (27). A transient tight-bouquet configuration then occurs in which homologs are largely synapsed. Fully synapsed chromosomes emerge from the bouquet at mid-pachytene, as stiff, straight units with ends once again dispersed throughout the nuclear periphery (as in mutant; Fig. 3*E*).

These observations divide the homolog pairing process into three successive morphological stages: (*i*) Recognition and rough, long-distance alignment of homologs; (*ii*) Presynaptic coalignment of homologs at a distance of ≈400 nm; and (*iii*) synapsis/SC formation. The first two stages precede entry of chromosome ends into a bouquet, and the third stage is concomitant with entry into, and presence of, the bouquet. Exit from the bouquet stage follows complete SC formation.

***ski8* Mutants and γ-Ray-Induced DSBs Define Three Mechanistically Distinct Stages of Homolog Juxtaposition.** 3D EM reconstructions show that type I mutants never proceed beyond the recognition stage of pairing (Fig. 5 *A* and *B*). At early leptotene, partial long-distance recognition of homologs is seen, similar to that seen at early WT leptotene (compare Figs. 5*A* and 6*B*). Neither presynaptic coalignment nor SC formation occur; instead, the early configuration persists until what would normally be pachytene, by ascus size. Type II mutants proceed farther: homologs are coaligned, with points of juxtaposition at the presynaptic alignment distance alternating with regions that are more separated (Fig. 5*C*); and sometimes an SC also forms (above). The difference between type I and type II mutants is dramatically apparent by Spo76-GFP staining (200 nuclei analyzed for each step). Homologs are obviously aligned only in type II (Fig. 5 *D* and *E*), with Rad51 foci often seen at sites of local presynaptic associations (Fig. 5 *F* and *G*), and complete or almost complete synapsis in 10–15% of the nuclei (above). Type I phenotypes are indistinguishable from those seen in *spo11*Δ (25), and *spo11*Δ *ski8-7* (type II) exhibits a *spo11*Δ phenotype (data not shown). All *ski8* mutants enter the bouquet configuration, but exit only after some delay, especially in type I mutants, as is also seen in *spo11* mutants (25).

These results suggest a direct relationship between the number of DSBs (indicated by Rad51 foci) and the extents of coalignment and SC formation. To further explore this relationship, we γ-irradiated *ski8* mutants at two doses, 200 and 100 Gy, at a stage when most nuclei are in early leptotene. In *spo11*Δ, a dose of 200 Gy promotes synapsis and chiasmata in ≈20% of nuclei that progress after irradiation (25). At 200 Gy, type I *ski8* mutants behave like *spo11* mutants. Type II mutants show greater restoration of synapsis: among 200 progressing nuclei examined after 7–8 h, ≈50% exhibited seven completely or partially synapsed bivalents (Fig. 5*H*), ≈35% exhibited one to three synapsed bivalents with remaining chromosomes not synapsed, and ≈15% exhibited broken/fragmented chromosomes (confirmed by DAPI). Before this point, 5–6 h after irradiation, nuclei of both types, like *spo11*Δ nuclei, exhibit essentially presynaptic coalignment (Fig. 5*I*). After exposure to 100 Gy, type I and type II mutants again exhibit strikingly different arrays of pairing configurations. The majority of progressing type I nuclei (200 examined) exhibited substantial presynaptic alignment (Fig. 5*J*); only 5% exhibited seven synapsed bivalents. Among 200 type II nuclei, 60% showed presynaptic alignment and 40% showed partial or complete synapsis (Fig. 5*K*). In effect, this lower level of γ-rays creates a type II phenotype in type I mutants, and a close-to-WT progression in type II mutants.

These observations suggest that DSBs are required for presynaptic coalignment and that an even higher level of DSBs is required for synapsis. Also, absence of presynaptic alignment and synapsis in *ski8* mutants is really due to an absence of DSBs, and not to any dominant interfering effect of the mutation itself.

***ski8* Mutations Alter Both Meiotic Divisions and Sporulation, as Do *spo11* Mutations.** *ski8* mutants exhibit segregation and spore-formation defects, analogous to those described for *spo11* mutants (25): random segregation of homologs at division I, delayed separation of sister chromatids at division II, and high levels of nonviable ascospores, e.g., 93 ± 8 for *ski8-7* to 127 ± 9 ascospores per perithecium for *ski8-33,* as compared with 810 ± 15 ascospores per perithecium for WT (30 counted per strain). γ-irradiation restores formation of asci containing eight viable ascospores, to ≈25% of all asci in each perithecium after 200 Gy treatment of a type II mutant, and to 5–10% in type I mutants.

***ski8* Mutations Suppress Prophase and Division I Defects of *spo76–1*, as Do *spo11* Mutations.** In a *spo76-1* mutant (21), meiotic chromosomes develop normally through mid-leptotene; then, at leptotene/zygotene, sister chromatids show split and fractured axes and chromosomes appear to be kinked. During the diffuse stage, sister cohesion is lost entirely such that only individual chromatids are seen at metaphase I, whereupon meiosis arrests. *spo11* mutations completely suppress *spo76-1* leptotene/zygotene axis and intersister defects, partially suppress loss of cohesion during the diffuse stage, and fully suppress metaphase I arrest. All of these defects reappear on irradiation of *spo11 spo76-1* mutants, implying that they are due to DSBs (25). *ski8* mutations confer the same *spo76-1* suppression effects as do *spo11* mutations. Suppression is less efficient in type II *ski8* mutants than in type I mutants, providing further evidence for greater and lesser levels, respectively, of DSBs. As a result, the number of ascospores per perithecium is 810 ± 15 in WT, 10^{-4} in *spo76-1*, 18 ± 2 in *spo76-1 ski8-7* (type II), and 49 ± 5 and 65 ± 8, respectively, in *spo76-1 ski8-33* and *spo76-1 ski8-13* (type I).

Discussion

Roles for Ski8p in the Vegetative and Sexual Cycles. Sordaria *ski8* mutants exhibit defects in vegetative growth, entry into the sexual cycle and during meiosis, but no DNA damage sensitivity. During meiosis, they exhibit severe defects in formation of Rad51 foci and chiasmata, and diverse additional defects identical to those of *spo11* mutants, all of which are restored by exogenously provided DSBs. Thus, Ski8p specifically promotes DSB formation in Sordaria.

Ski8p Exhibits Meiosis-Specific Nuclear and Chromosomal Localization in Temporal and Functional Coordination with Spo11p. Ski8p localizes to the cytoplasm in all cells of the vegetative and sexual cycles. In its roles for RNA metabolism, Ski8p works in a tight complex with Ski2 and Ski3 proteins, both of which are cytoplasmically localized (6). General cytoplasmic Ski8p localization could reflect a role in RNA metabolism also for Sordaria.

Ski8p also occurs in nuclei, over the chromosomes, specifically during earl-mid-meiotic prophase, with exactly the same timing as Spo11p. Moreover, normal localization of Ski8p and Spo11p are mutually interdependent. Spo11-modulated localization of Ski8p to meiotic nuclei has also been seen in *Saccharomyces cerevisiae* (C. Arora and S. Keeney, personal communication). These results suggest that Ski8p mediates DSB formation directly, by affecting meiotic prophase chromosomes, rather than indirectly, e.g., by means of effects on RNA metabolism and thus on expression of Spo11p or another DSB-related protein. Phys-

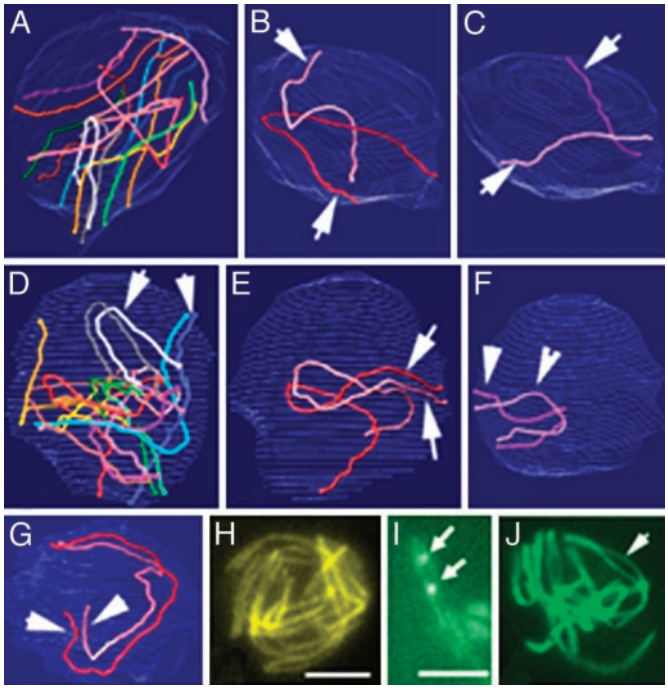

Fig. 4. Progressive colocalization of homologs in WT. (*A–G*) 3D EM reconstructions of three serially sectioned nuclei. (*A–C*) Early leptotene nucleus. (*A*) The seven homologs are represented with matching colors. (*B*) Homolog pair 1 (arrows). (*C*) Pair 7 (arrows). These two pairs are easy to distinguish by their size. They show no sign of pairing. (*D–F*) Mid-leptotene nucleus with partially aligned homologs (arrows). (*D*) Overview. (*E*) Pair 1 shows only telomere alignment (arrows). (*F*) The small pair 7 is completely aligned. (*G*) At late leptotene, all homologs are completely aligned, illustrated here by pair 1 (arrows). (*H*) LM of equivalent nucleus (axes are stained by Spo76-GFP). (*I*) Two pairs of homologs (stained by Spo76-GFP) show Rad51-GFP foci (arrows) between the aligned axes. (*J*) Zygotene nucleus with partially synapsed bivalents (arrow) and telomeres grouped into a bouquet configuration. (Bars, 5 μm for LM and 1 μm for EM.)

ical interaction between Ski8p and Spo11p could be involved (19). Ski8p is required for DSB formation even when Spo11p is targeted artificially to a specific binding site (17); thus, its effect may not be on localization of Spo11p alone. As Spo11p remains located in the nucleus in a *ski8* mutant, but diffusely, an interesting possibility is that Ski8p mediates the formation of higher-order chromatin features that promote DSB formation within assembled Spo11p complexes. Ski8p (and Spo11p) could also have post-DSB roles: both proteins remain on the chromosomes well after DSB formation; budding yeast Ski8p interacts with Rdh54/Tid1 (29), which likely acts after DSB formation (30), and Spo11p negatively regulates bouquet exit (25).

Why is Ski8p involved in both RNA processing and meiotic DSB formation? It could be recognizing RNA components of meiotic chromosomes. Alternatively, the WD repeat motifs of Ski8p may be a scaffold that brings together different or partially overlapping sets of proteins in its two roles. A scaffolding role could be useful in promoting higher-order chromatin assemblies.

Meiotic DSBs Mediate Presynaptic Coalignment of Homologs. DSBs are required for presynaptic homolog coalignment, which, in Sordaria, can be promoted by either programmed or exogenous DSBs (this article and ref. 25). The current results suggest that DSBs modulate this process. Rad51 occurs on and between the axes of presynaptically coaligned homologs in Sordaria, as well as in other organisms (28). The extent of coalignment directly correlates with the level of DSBs or Rad51 foci, and, at suboptimal DSB levels, individual points of association become apparent, with Rad51 foci often seen at those same positions. DSB-dependent, SC-independent close homolog juxtaposition is also detected by Lox/Cre recombination in budding yeast (31). How could DSBs, which occur within chromatin loops (32), mediate presynaptic coalignment of homologs? Meiotic recombination complexes become associated with their underlying chromosome axes before or immediately after post-DSB formation (32, 33). The DSB within an axis-associated post-DSB recombination complex might first identify, and then form a stable association with, the homologous sequence present in the corresponding chromatin loop of its homolog. The recombination complex might then reel in the partner axis by tracking along that captured loop. Once the partner axis comes within reach, an

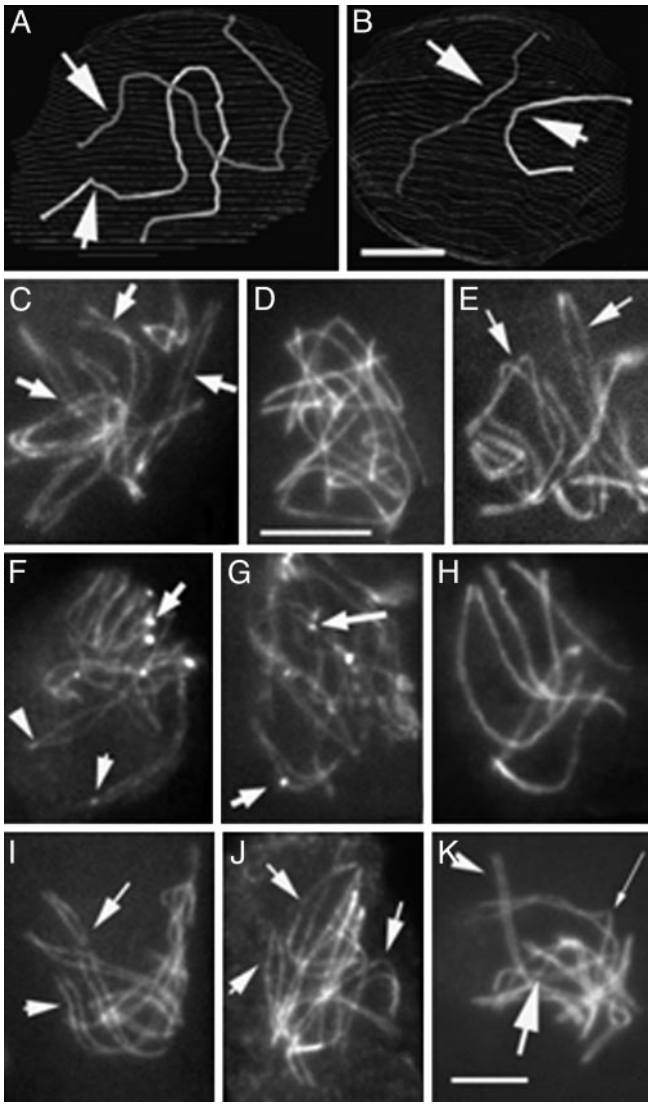

Fig. 5. Stages of homolog juxtaposition in mutants. (*A* and *B*) EM reconstruction of a *ski8-33* (type I) nucleus. Homologs of pair 1 (*A*) and 7 (*B*) show only long distance partial recognition segments (arrows). (*C–K*) Spo76-GFP staining. (*C*) *ski8-7* nucleus with clear homologous alignment (arrows point to three pairs). Type I *ski8-34* (*D*) shows no alignment, whereas type II *ski8-22* (*E*) does (arrows point to two pairs). (*F* and *G*) Spo76-GFP and Rad51-GFP (arrows) double-stained *ski8-7* (*F*) and *ski8-22* (*G*) nuclei. (*H* and *I*) Exposure at 200 Gy. (*H*) Complete synapsis in *ski8-7* after 8 h. (*I*) Homolog alignment in *ski8-33* (arrows) after 6 h. (*J* and *K*) Exposure at 100 Gy. (*J*) *ski8-33* nucleus with aligned homologs (arrows). (*K*) *ski8-22* nucleus shows a mixture of synapsed (arrowhead), aligned (thin arrow), and still roughly aligned (large arrow) homologs. (Bars, 5 μm for LM and 1 μm for EM.)

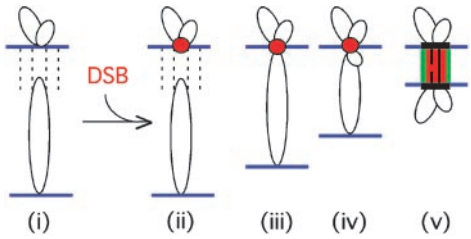

Fig. 6. Model for DSB-mediated presynaptic axis coalignment. Homologs linked by DSB-independent homolog recognition (*i*) undergo a DSB. A DSB within an axis-associated recombination complex (red ball) captures the homologous sequence of a partner chromatin loop (*ii*) and reels the partner axis into close range by tracking along the partner loop (*iii* and *iv*), thus permitting formation of an interaxis structural bridge overlaid with a nascent DSB/partner/RecA homolog complex (*v*).

appropriate link is made, which joins homolog axes at the presynaptic alignment distance (ref. 25 and Fig. 6).

SC Formation Requires More DSBs Than Does Presynaptic Coalignment, and More Than One DSB Per Chromosome. DSBs promote SC formation (above and ref. 3). We now find that intermediate levels of DSBs give only coalignment, with higher levels required for segments of synapsis (SC). SC formation appears to be nucleated at sites of recombination interactions that eventually mature into crossovers (ref. 1; K. A. Henderson and S. Keeney, personal communication; for Sordaria, see ref. 27). Only a subset of DSBs give rise to crossovers, approximately one-third in Sordaria (A.S. and D.Z., unpublished work). Thus, our results are explained if every DSB can promote coalignment of the corresponding axis regions, whereas only the DSBs that yield crossovers can nucleate SC formation.

In type II mutants and in type I mutants after 100 Gy irradiation, only partial SC is seen. Thus, nucleation of SC at a single site does not permit polymerization along the entire chromosome. Analogously, in Sordaria *asy2–17*, crossing over is reduced by half and synapsis is incomplete, but each individual segment of SC is still accompanied by a single crossover-correlated recombination nodule (27). What prevents nucleated SC from polymerizing indefinitely? Designation of a particular recombinational interaction as a crossover is accompanied by interference, which disfavors designation of additional crossovers nearby. This effect spreads outward from its initial starting point for a certain distance in both directions. Most interference models suppose that information is transmitted along chromosome axes; further, we favor the view that crossover interference precedes SC formation (34, 35). We therefore propose that interference licenses SC polymerization.

Three Mechanistically Distinct Stages of Meiotic Homolog Juxtaposition. Progressive juxtaposition of homologs during meiotic prophase is accomplished by three mechanistically distinct processes that occur in overlapping succession and can be differentiated by their dependencies on DSBs (above, and refs. 24, 25, and 31). Stage I: DSB-independent partial homolog recognition. Some segments or homolog pairs are placed into joint spaces in the nucleus, as seen in early leptotene of WT meiosis and in DSB-defective mutants (*spo11* and *ski8* type I). This process may minimize creation of entanglements by later DSB-mediated interactions. Stage II: DSB-dependent presynaptic coalignment of homologs at ≈400 nm. Stage III: SC formation. Nucleation at sites of future crossovers is followed by limited spreading outward along the chromosomes. In Sordaria, stage I, and stage II pairing are achieved before colocalization of chromosome ends in a bouquet, and the bouquet stage then occurs concomitant with stage III (synapsis).

We thank Françoise James for assistance and Scott Keeney for discussions and generous sharing of prepublication results. This work, A.S., and S.T., were supported by Centre National de la Recherche Scientifique Grant UMR8621 (to D.Z.) and National Institutes of Health Grant GM25326 (to N.K.). S.G. was supported by Ministero dell'Universitá e della Ricerca Scientifica e Tecnologica-Consiglio Nazionale delle Ricerche Program *lex* 488/92 Cluster 02.

1. Zickler, D. & Kleckner, N. (1999) *Annu. Rev. Genet.* **33,** 603–754.
2. Lee, J. Y. & Orr-Weaver, T. L. (2001) *Annu. Rev. Cell Dev. Biol.* **17,** 753–777.
3. Keeney, S. (2001) *Curr. Top. Dev. Biol.* **52,** 1–53.
4. Paques, F. & Haber, J. E. (1999) *Microbiol. Mol. Biol. Rev.* **63,** 349–404.
5. Ridley, S. P., Sommer, S. S. & Wickner, R. B. (1984) *Mol. Cell. Biol.* **4,** 761–770.
6. Brown, J. T, Bai, X. & Johnson, A. W. (2000) *RNA* **6,** 449–457.
7. Araki, Y., Takahashi, S., Kobayashi, T., Kajiho, H., Hoshino, S. & Katada T. (2001) *EMBO J.* **20,** 4684–4693.
8. Jacobs Anderson, J. S. & Parker, R. (1998) *EMBO J.* **17,** 1497–1506.
9. Masison, D. C., Blanc, A., Ribas, J. C., Carroll, K., Sonenberg, N. & Wickner, R. B. (1995) *Mol. Cell. Biol.* **15,** 2763–2771.
10. van Hoof, A., Staples, R. R., Baker, R. E. & Parker, R. (2000) *Mol. Cell. Biol.* **20,** 8230–8243.
11. Smith, T. F., Gaitatzes, C., Saxena, K. & Neer, E. J. (1999) *Trends Biochem. Sci.* **24,** 181–185.
12. Matsumoto, Y. G., Sarkar, S., Sommer, S. & Wickner, R. B. (1993) *Yeast* **9,** 43–51.
13. Malone, R. E., Bullard, S., Hermiston, M., Rieger, R., Cool, M. & Galbraith, A. (1991) *Genetics* **128,** 79–88.
14. Evans, D. H., Li, Y. F., Fox, M. E. & Smith, G. R. (1997) *Genetics* **146,** 1253–1264.
15. Fox, M. E. & Smith, G. R. (1998) *Prog. Nucleic Acid Res. Mol. Biol.* **61,** 345–378.
16. Gardiner, J. M., Bullard, S. A., Chrome, C. & Malone, R. E. (1997) *Genetics* **146,** 1265–1274.
17. Pecina, A., Smith, K. N., Mezard, C., Murakami, H., Ohta, K. & Nicolas, A. (2002) *Cell* **111,** 173–184.
18. Deveaux, L. C., Hoagland, N. A. & Smith, G. R. (1992) *Genetics* **130,** 251–262.
19. Uetz, P., Giot, L., Cagney, G., Mansfield, T. A., Judson, R. S., Knight, J. R., Lockshon, D., Narayan, V., Srinivasan, M., Pochart, P., *et al*. (2000) *Nature* **403,** 623–627.
20. Huynh, A. D., Leblon, G. & Zickler, D. (1986) *Curr. Genet.* **10,** 545–555.
21. van Heemst, D., James, F., Pöggeler, S., Berteaux-Lecellier, V. & Zickler, D. (1999) *Cell* **98,** 261–271.
22. Pöggeler, S., Nowrousian, M., Jacobsen, S. & Kück, U. (1997) *J. Microbiol. Methods* **29,** 49–61.
23. Thompson-Coffe, C. & Zickler, D. (1993) *J. Cell Sci.* **104,** 883–898.
24. Zickler, D. (1977) *Chromosoma* **61,** 289–316.
25. Storlazzi, A., Tessé, S., Gargano, S., James, F., Kleckner, N. & Zickler, D. (2003) *Genes Dev.* **17,** in press.
26. Bishop, D. K. (1994) *Cell* **79,** 1081–1092.
27. Zickler, D., Moreau, P. J., Huynh, A. D. & Slezec, A. M. (1992) *Genetics* **132,** 135–148.
28. Tarsounas, M., Morita, T., Pearlman, R. E. & Moens, P. B. (1999) *J. Cell Biol.* **147,** 207–220.
29. Ito, T., Chiba, T., Ozawa, R., Yoshida, M., Hattori, M. & Sakaki, Y. (2001) *Proc. Natl. Acad. Sci. USA* **98,** 4569–4574.
30. Shinohara, M., Gasior, S. L., Bishop, D. K. & Shinohara, A. (2000) *Proc. Natl. Acad. Sci. USA* **97,** 10814–10819.
31. Peoples, T. L., Dean, E., Gonzalez, O., Lambourne, L. & Burgess, S. M. (2002) *Genes Dev.* **16,** 1682–1695.
32. Blat, U., Protacio, R. U., Hunter, N. & Kleckner, N. (2002) *Cell* **111,** 1–12.
33. van Heemst, D. & Heyting, C. (2000) *Chromosoma* **109,** 10–26.
34. Storlazzi, A., Xu, L., Schwacha, A. & Kleckner, N. (1996) *Proc. Natl. Acad. Sci. USA* **93,** 9043–9048.
35. Hunter, N. & Kleckner, N. (2001) *Cell* **106,** 59–70.